

CHEMICAL ASPECTS OF THE IMPACT PROCESS

Introduction, Rationale, and Purpose:

Impact cratering, as arguably the only geological process common to all solid bodies in the Solar System, plays an integral role in the formation and evolution of planetary systems [1, 2, 4, 6, 7]. For the past few decades, studies of impact cratering have focused primarily on constraining physical aspects of the impact process. However, in recent years it has been recognized that the impact process leaves not only physical traces but also chemical signatures. Anomalous concentrations of several elements have been found at impact sites around the globe (e.g. Chicxulub, Vredefort, and Sudbury). The best-known chemical signature of impact is perhaps the anomalous concentration of iridium found at the Cretaceous-Tertiary boundary.

Though it is now generally accepted that the impact process leaves distinct chemical signatures, the mechanism by which such chemical signatures are formed has not been well characterized.

An understanding of the chemical processes occurring during the impact process is essential if field-based geochemical applications relying on impact-induced chemical anomalies are to progress (e.g. post-impact identification of impactor type). An understanding of the chemical aspects of the impact process is also essential to answering fundamental questions about the formation and evolution of planetary systems and may yield clues to the origins of terrestrial life [2, 6, 7].

The goal of my study is to characterize the behavior of trace elements during the impact process, thereby allowing the elucidation of principles governing the mobility and behavior of trace elements during an impact event. Experimentally induced impacts, such as those employed in this investigation, are important to the study of the impact process because the conditions of

the impact event can be closely controlled. Experiments are crucial to the study of the chemistry of the impact process because the composition of the target material before and after impact can be accurately and precisely measured, eliminating the complication of determining the indigenous component of an impact site in the field [5].

General Background:

The impact process is characterized by high temperatures (>2000° C) and extreme pressures (tens to hundreds of gigapascals) and consists of three major phases: compression, excavation, and modification.

During the compression phase, intense hemispheric shock waves radiate outward from the point of impact, compressing and deforming the target material, usually past its Hugoniot elastic limit. During this phase, material near the point of impact is vaporized; material in the nearby vicinity is melted.

During the excavation stage of the impact

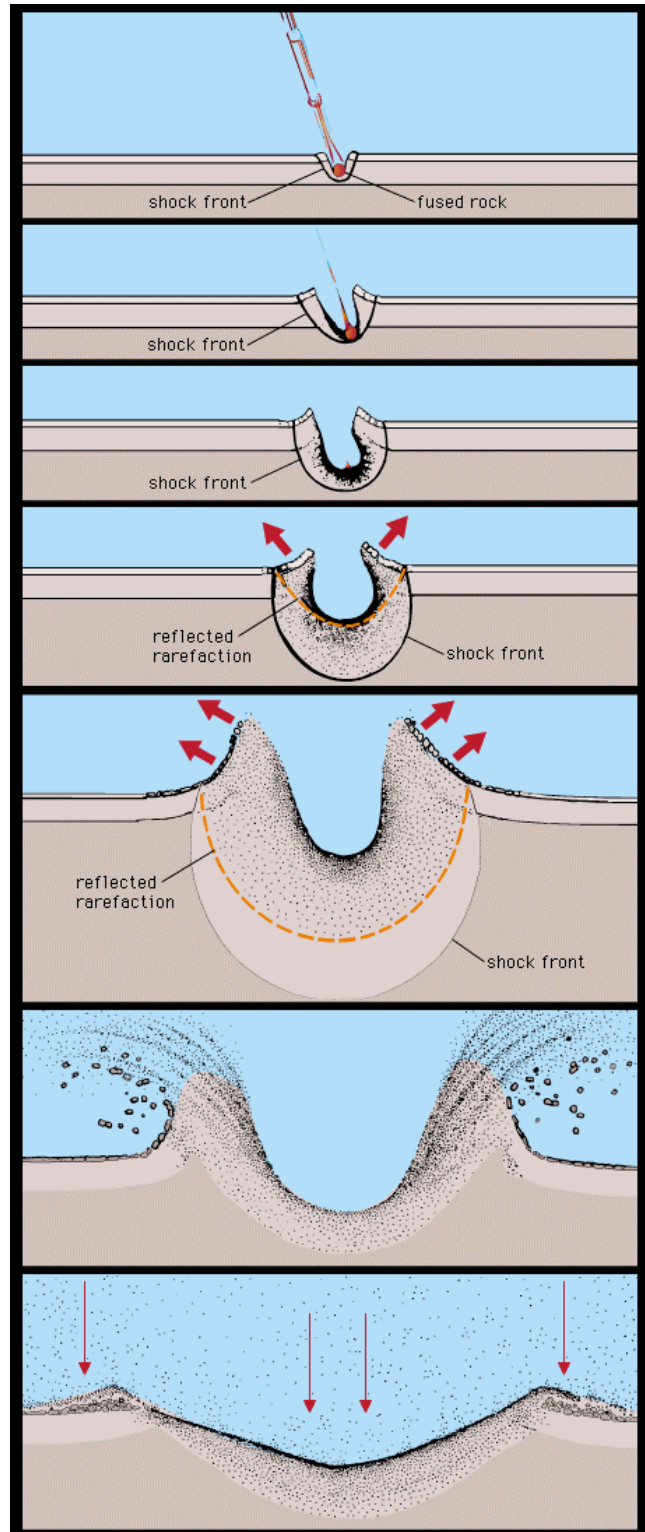


Figure 1: A simplified diagram illustrating the impact process. The first three segments depict the compression stage; the next three segments the excavation stage, and the final segment the modification stage. Courtesy of University of Oregon.

process, a rarefaction wave passes back through the target material, unloading almost instantaneously the intense pressure exerted by the passage of the shock wave(s). This rapid unloading of pressure results in melting of some mineral grains. This melting process is not the eutectic process commonly seen in petrological systems, but rather a spontaneous and complete melting of entire mineral grains. As the rarefaction wave propagates back through the target material, it excavates the crater, throwing rock, dust, and melt into the atmosphere, forming the vapor plume/ejecta curtain.

The modification phase occurs as the ejecta falls back to the ground and the crater relaxes to its final shape. See figure 1 [1, 2, 4, 7].

Pertinent Literature:

Detailed isotopic analyses of impact ejecta have allowed the correlation of certain meteorite types to specific impact craters, techniques pioneered by Koeberl and Tagle [5, 13]. Though both Koeberl and Tagle have been able to correlate the chemical signatures found at specific impact sites to the chemical and isotopic composition of specific meteorite types, neither has cohesively described the mechanism by which chemical signatures are incorporated into the ejecta. The work of Koerbel and Hagle does, however, strongly suggest that the chemical signature left by an impact event is dependent on the composition of the impacting body.

A recent paper by Ebel and Grossman “predict[s] for the first time the sequential condensation of solids and liquids from the plume of vaporized rock expected from oblique K-T impacts. . . . [and] predict[s] highly oxidizing plumes that condense silicate liquid droplets bearing spinel grains. . . . [3].

The 2005 International Conference on Impact Cratering featured a presentation by Melosh, who emphasized the lack of attention given to chemical aspects of the impact process and gave

an overview of scientists' limited understanding of the chemical aspects of the impact process [8].

Concurrent Work:

At the time this research was conducted, I was the only researcher studying the chemical aspects of the impact process at the labs where my study was conducted. A few other researchers around the globe (e.g. [3, 5, 8, 11, 12], etc.) are in the midst of experiments, simulations, and fieldwork studying varying facets of the chemical processes occurring during the impact process. None of these individuals were involved in the design or execution of my study, although one individual facilitated the use of equipment (see methodology section); others were asked to peer review my study.

Methodology:

A sample of granite was taken from the Silver Plume Batholith in Colorado, USA. The sample was fresh as it was taken after penetrating approximately 20 cm into the rock body; the sample was then broken into 48 smaller pieces (approximately 500 g each) for ease of transport and handling. Throughout this paper, *sample* will refer to the collective smaller pieces and *specimen* to the individual pieces broken off the sample. It is imperative to realize that because all specimens are pieces of the original sample, they are as mineralogically and chemically homogeneous as possible. The specimens were randomly designated as a control or experimental individual using standard SRS (simple random sampling) technique.

Ten control specimens were analyzed using x-ray fluorescence (XRF) and inductively-coupled plasma mass spectrometry (ICP-MS). Samples were prepared using a fused-bead procedure in a HEPA clean room. Concentrations of Ni, Cr, Sc, V, Rb, Sr, Zr, Y, Nb, Ga, Cu, Zn, Pb, La, Ce, Nd, U, Pr, Sm, Eu, Gd, Tb, Dy, Ho, Er, Tm, Yb, Lu, Ba, Th, Hf, Ta, and Cs were

quantitatively measured. The mean concentration of each element was calculated. See Table 1.

Impact events were induced using a two-stage light gas gun. An aluminum bead 6.35 mm in diameter was fired into an experimental specimen at approximately 5.53 km s^{-1} at an angle 90° from the horizontal in a vacuum of 0.19 torrs. The interior of the impact chamber was approximately one meter in diameter and was marked off into four quadrants. Ejecta from the impact event were collected using techniques to minimize contamination; each piece of ejecta was individually collected with forceps and placed in a sterile container after recording in which quadrant it was found; in addition, the impact chamber was thoroughly cleaned prior to, and in between, the experiments discussed in this paper.

Ejecta material was then sent for XRF and ICP-MS analysis and was prepared under the exact same conditions, using the same protocols, as were the control samples. Ejecta from the same quadrant were analyzed together. The mean concentration for each element was calculated. See Table 1. Because both the control and experimental samples were prepared using the same techniques, in the same environment, contamination was minimized. Since conditions, calibration, and procedures were identical for both control and experimental specimens, any contamination that occurred is the same for both sets of specimens, allowing a valid statistical comparison of the concentrations of elements in the control specimens with those in the experimental specimens.

Standard 0.03 mm-thick, one-inch diameter thin sections were made of both control and experimental samples. The thin sections from both samples were analyzed and compared under plane- and crossed-polarized light. Each thin section was also chemically mapped using a scanning electron microscope equipped with an energy-dispersive spectrometer (SEM/EDX).

Aluminum beads from the same stock as those used in the experimental impact events that

were part of my study were analyzed using glow discharge mass spectrometry (GDMS) in clean room conditions. The projectile was found to be mostly aluminum, with about 5% Cu, 8690 ppm Mg, 6050 ppm Si, 5525 ppm Mn, 6050 ppm Fe, 2200 ppm Zn, and 27 ppm Ni.

Analysis:

Part I: Analysis of XRF/ICP-MS Data: XRF and ICP-MS were used to determine the concentration of trace elements in both control and experimental specimens. XRF detected Sc, V, Ni, Cr, Ba, Sr, Zr, Y, Rb, Nb, Ga, Cu, Zn, Pb, La, Ce, Th, and Nd; ICP-MS detected the fourteen naturally occurring REEs, Ba, Th, Nb, Y, Hf, Ta, U, Pb, Rb, Cs, Sr, Sc, and Zr. For those elements that were detected by both XRF and ICP-MS, the values from ICP-MS were used. In order to compare the concentration of a given trace element in the control specimens to the concentration of that same element in experimental specimens, various statistical techniques were employed.

A spidergram was made to compare the mean concentration of each element in the control specimens to the concentration of the same element in the experimental specimens (figure 2). Each point on the spidergram was calculated by dividing the experimental mean of an element by the control mean of that same element.

Points that stray away from the

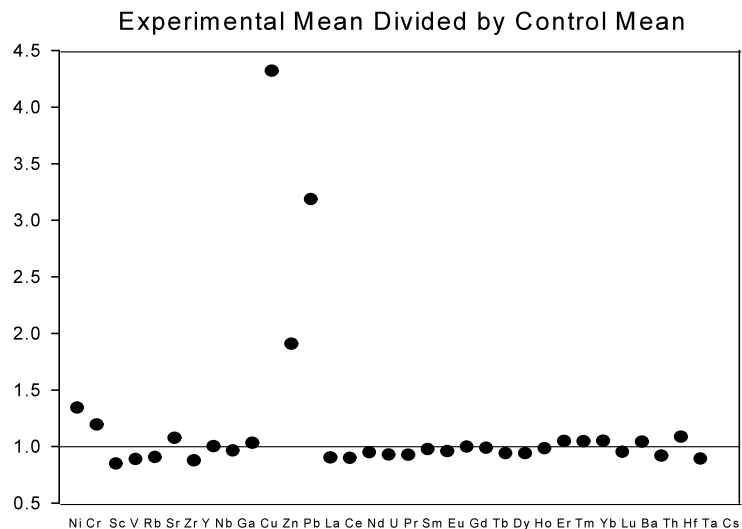


Figure 2: Each point represents the quotient of the experimental mean and the control mean. Elements whose point falls away from the line $y=1$ may have a concentration in the experimental specimens that is significantly different from the concentration in the control specimens. The further a point is from the line, the stronger the evidence that the concentration of that element in the experimental specimens is different from the concentration of that element in control specimens

line $y = 1$ indicate that the concentration of that element may be significantly different in the experimental specimens than in the control specimens. As the distance between the line and an element's point increases, the strength of the evidence that the concentration of that element in the experimental specimens is different from the concentration of that element in the control specimens increases. A point that lies below the line indicates that the experimental specimens have a lower concentration of the element than is found in the control specimens; that is, an element whose point falls below the line is said to be depleted in the experimental specimens. Similarly, an element whose point falls above the line indicates that the experimental specimens have a higher concentration of that element than do the control specimens; these elements are enriched in the experimental specimens compared to the control specimens.

In addition to the spidergram, boxplots, normal quantile plots, and histograms were constructed for each element and were interpreted to determine characteristics of the distribution of both the control and experimental data. Analysis of these graphs indicated that the distribution of the concentration of an element in the ten control specimens was approximately normal, while the distribution of the concentration of an element in the experimental specimens was clearly non-normal.

I used modern resampling techniques (e.g. bootstrapping, jackknifing, permutation tests, etc.) to statistically analyze my data because the P-values and confidence intervals given by such methods are more accurate than t -procedures. Instead of relying on theoretical sampling distributions, resampling techniques approximate the sampling distribution of a statistic using the data itself, removing the need for heavy statistical theory [10].

Two bootstrapping BCa confidence intervals (10,000 replications) at $C = 0.05$ were constructed for each element, one by using the control data and the other generated using the

experimental data. Comparison of these confidence intervals allows significant differences between the control and experimental groups to be detected. See Table 1. A permutation test (999,999 resamples), a hypothesis test based on resampling, was used to compare the concentration of each element in the experimental and control specimens. P-values given by the permutation test were used, in combination with BCa confidence intervals and EDA, to make a decision about the significance of the chemical data. See Table 1.

Based on statistical evidence, I am highly confident that the concentration of Cu ($P = 0.003$), Ni ($P = 0.041$), Pb ($P = 0.001$), Zn ($P = 0.001$), Rb ($P = 0.012$), and Sc ($P = 0.035$) is of a significantly different concentration in the experimental specimens than in the control specimens.

Part II: Analysis of Thin Sections: Standard round thin sections were made from both control and experimental specimens. I then analyzed these thin sections under plane- and cross-polarized light to determine the extent to which the impact process deformed/metamorphosed the target granite. Extensive analysis of the thin section made from impact ejecta showed severe deformation

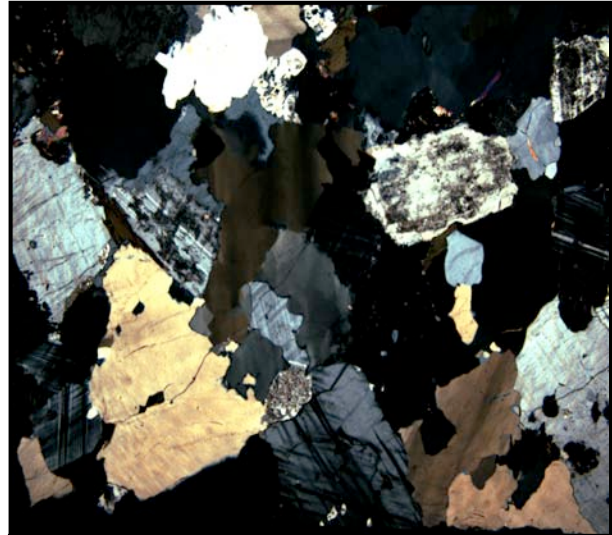


Figure 3: Micrograph of the control thin section taken under cross-polarized light at 20x. Note the clean mineral boundaries and generally unstrained nature of the crystals. (The plagioclase in the upper right is rather deformed, but the other minerals are relatively unmodified.)

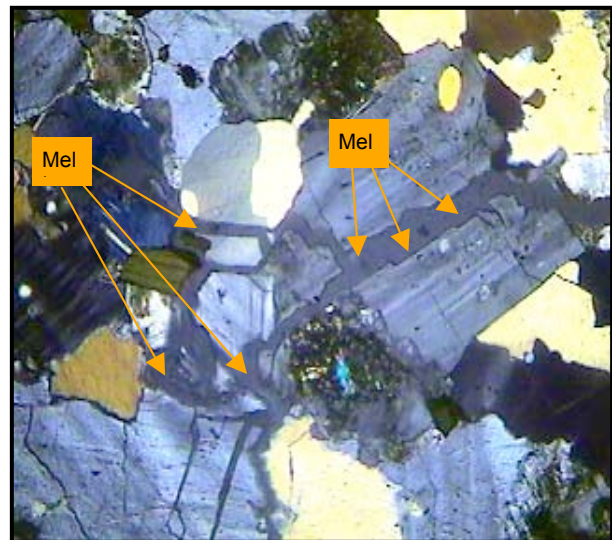


Figure 4: Micrograph of the experimental thin section taken under cross-polarized light at 20x. Note the melt system that breaks up crystal faces and intrudes into interstitial boundaries. Also, note the fracture systems seen in several of the minerals in this field.

features and melt systems, suggesting that shock pressures up to tens of gigapascals were reached [9]. Analysis indicates that mineral lattices were severely deformed during the impact event. See Figures 3, 4, and 5 (taken under cross-polarized light at 20x). Figure 3 is an image of part of the control thin section; figures 4 and 5 are parts of the experimental thin section. Melt systems were observed to cut across crystal faces as well as along interstitial

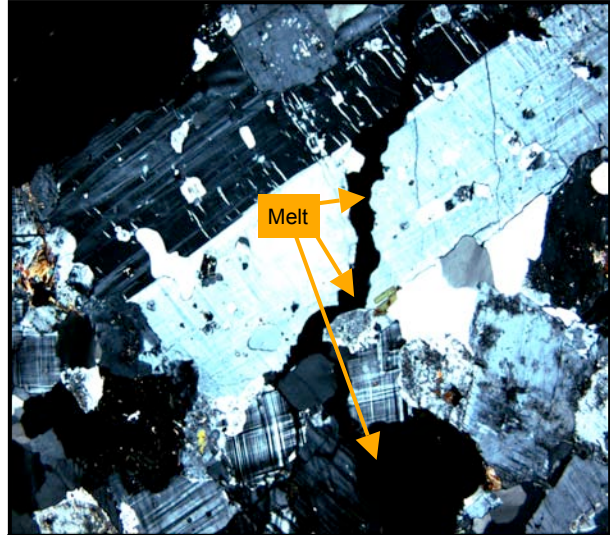


Figure 5: Micrograph of the experimental thin section taken under cross-polarized light at 20x. Note the dark band cutting across the crystal in the center of the image. Such bands are melt glasses. Note also the fracture systems and stress features seen in the crystals.

boundaries. Individual minerals were broken into fragments by the shock pressures of the impact event and melt intruded into the resulting fracture systems. It is important to note that the melting of minerals in the impact process is not the eutectic process found in most petrological systems, but rather an instantaneous process in which entire mineral grains melt spontaneously and completely [4].

Part III: Analysis of SEM/EDX Data: I mapped the thin sections using SEM/EDX to determine the abundance of major elements. The maps were particularly useful for mapping the abundance of aluminum, the main component of the projectiles used to induce impact.

Results:

Analysis of thin sections indicates that the target material was subjected to pressures of tens of gigapascals. Mineral assemblages exhibit severe deformation features and complex melt systems. The complex melt assemblages likely consist of a combination of target and projectile material.

Statistical evidence strongly suggests that Ni, Cu, Zn, and Pb were enriched in experimental specimens, while Sc and Rb were depleted. The melt systems and deformation features seen in thin section likely played a role in changing the concentrations of these elements.

| Table 1: Summary of Statistical Analyses of Chemical Data | | | | | | | |
|---|------------------|-----------------|---------|--------------|---------|-------------|---------|
| | Ctrl. Mean (ppm) | Exp. Mean (ppm) | P-Value | Ctrl: 95% CI | | Exp: 95% CI | |
| Ni | 6.400 | 8.600 | 0.041 | 5.700 | 7.100 | 6.667 | 10.250 |
| Cr | 6.700 | 8.000 | 0.411 | 5.500 | 8.600 | 6.200 | 10.500 |
| Sc | 4.600 | 3.900 | 0.035 | 4.207 | 5.240 | 3.716 | 4.080 |
| V | 14.400 | 12.800 | 0.164 | 13.300 | 15.900 | 12.167 | 13.667 |
| Rb | 216.270 | 196.240 | 0.012 | 207.210 | 224.195 | 191.616 | 201.335 |
| Sr | 145.910 | 157.090 | 0.073 | 140.173 | 152.865 | 150.205 | 166.570 |
| Zr | 189.990 | 166.710 | 0.086 | 173.833 | 218.526 | 164.415 | 170.363 |
| Y | 29.450 | 29.540 | 0.965 | 26.313 | 33.224 | 28.408 | 32.000 |
| Nb | 13.260 | 12.780 | 0.404 | 12.765 | 13.871 | 11.988 | 13.930 |
| Ga | 18.200 | 18.800 | 0.444 | 17.600 | 18.900 | 18.200 | 19.667 |
| Cu | 10.600 | 45.800 | 0.003 | 7.300 | 15.500 | 26.333 | 85.750 |
| Zn | 49.700 | 94.800 | 0.001 | 46.800 | 52.800 | 72.044 | 125.500 |
| Pb | 27.120 | 86.440 | 0.001 | 18.583 | 35.819 | 60.320 | 112.028 |
| La | 65.410 | 59.080 | 0.631 | 57.279 | 79.624 | 54.750 | 63.823 |
| Ce | 122.860 | 110.500 | 0.520 | 108.791 | 146.478 | 101.580 | 119.657 |
| Nd | 43.140 | 40.900 | 0.774 | 38.405 | 51.237 | 37.790 | 43.850 |
| U | 5.550 | 5.160 | 0.741 | 4.407 | 7.033 | 4.886 | 5.303 |
| Pr | 12.400 | 11.490 | 0.701 | 11.007 | 14.826 | 10.580 | 12.350 |
| Sm | 8.000 | 7.820 | 0.848 | 7.285 | 9.122 | 7.298 | 8.285 |
| Eu | 0.980 | 0.940 | 0.577 | 0.921 | 1.059 | 0.908 | 0.980 |
| Gd | 5.860 | 5.850 | 0.994 | 5.372 | 6.399 | 5.553 | 6.143 |
| Tb | 0.860 | 0.850 | 0.899 | 0.783 | 0.929 | 0.798 | 0.893 |
| Dy | 4.820 | 4.530 | 0.469 | 4.357 | 5.339 | 4.354 | 4.823 |
| Ho | 0.970 | 0.910 | 0.546 | 0.862 | 1.100 | 0.878 | 0.995 |
| Er | 2.780 | 2.740 | 0.555 | 2.459 | 3.167 | 2.638 | 2.992 |
| Tm | 0.450 | 0.470 | 0.627 | 0.394 | 0.506 | 0.450 | 0.520 |
| Yb | 3.030 | 3.170 | 0.625 | 2.692 | 3.386 | 3.060 | 3.510 |
| Lu | 0.510 | 0.530 | 0.588 | 0.455 | 0.563 | 0.518 | 0.560 |
| Ba | 713.630 | 680.430 | 0.590 | 646.709 | 800.240 | 665.885 | 699.060 |
| Th | 33.250 | 34.690 | 0.710 | 28.304 | 36.457 | 30.692 | 40.134 |
| Hf | 5.870 | 5.400 | 0.191 | 5.503 | 6.494 | 5.293 | 5.478 |
| Ta | 1.370 | 1.490 | 0.463 | 1.183 | 1.561 | 1.376 | 1.648 |
| Cs | 5.480 | 4.890 | 0.146 | 5.050 | 6.212 | 4.603 | 5.027 |

Table 1: This table summarizes the statistical inference performed on the chemical data given by XRF and ICP-MS. Ctrl. stands for the control specimens; Exp. stands for the experimental specimens. P-values were generated using a permutation test; confidence intervals were generated using the bootstrapping BCa method.

Discussion:

The impact process is isentropic, meaning that temperature and pressure vary together. In comparison, most petrologic systems maintain a constant pressure or temperature while the other varies. The isentropic nature of the impact process makes the chemical processes occurring during the impact process radically different from those occurring in standard petrological systems. Another constraint on the chemical processes occurring during an impact event is time; in all but the largest events, the compression phase lasts for only a few milliseconds. The modification stage is completed in a few minutes. All of these factors restrict the conditions that govern the chemical processes occurring during an impact event.

Based on geochemical data and thin section analyses, I propose the following model of the behavior of trace elements in the impact process at melt/solid boundaries, describing the kinetic and thermodynamic processes by which chemical signatures are formed.

When an impact event occurs, extreme temperatures and pressures are transiently exerted on both the projectile and target material. After shock wave(s) pass through both the projectile and target, rarefaction wave(s) swiftly unload the pressure exerted by the shock wave(s), causing in melting of both target material and the projectile. Melts of the target were seen observed in my analysis of the experimental thin section. See figures 3-5. Since the pressures exerted by the shock wave decay by a power law relative to the radius of the projectile, most of the projectile and a portion of the target material near the impact point melt, and may vaporize depending local T/P conditions. Thus, the amount of melt that is formed from an impact can be expressed as a function of distance from the impact point. Moreover, since the projectile is at the impact point, the projectile is mostly melted. The melted projectile and melted target mix. As the projectile/target melt mixture intrudes fracture systems in the mineral assemblages (caused by

the passage of the shock wave(s)), the incorporation of chemical components takes place at melt/solid boundaries. Based on this model, it makes sense that the experimental data did not follow a normal distribution, even though the control data did approximate a normal distribution. Indeed, the graphs of the experimental data were strongly skewed. This skewness can be accounted for if the volume of melt intruded into the fracture systems is a function of distance from the impact point; the chemical anomalies seen would be less pronounced as the distance between the impact point and the site of analysis increases. Ejecta were collected by quadrant, and high-speed video of the impact event itself showed that ejecta from the same part of the specimen were distributed throughout the impact chamber because of ricochet. It is likely that the samples that were chemically analyzed came from different parts of the original specimen, and therefore were located at different distances from the point of impact and thus experienced varying T/P conditions and interaction with the mixed target/projectile melt. There is no way to actually trace the location of each piece of ejecta because of the ricocheting action inside the impact chamber and so I am unable to verify this hypothesis at this time, but further experiments will help determine the validity of this supposition. Therefore, I propose that the intensity of chemical anomalies can be expressed as a function of distance from the impact point, an idea that is supported by the skewness of the experimental data. Something had to happen to make the experimental data skewed since the control data was approximately normal; an environment in which the intensity of the chemical changes can be expressed as a function of distance could account for the skewness of my experimental data.

Farther away from the point of impact, individual mineral species may melt after the passage of the rarefaction wave, but not to the extent that those grains nearer the point of impact will. Near the point of impact, the melt of the target and projectile mix. Minerals are fractured and

stressed; the melt, which is a mixture of projectile melt and target melt, intrudes some of these cracks and interstices, forming the glasses seen inside of the fracture systems that are visible in the experimental thin section. See figures 4 and 5. Since the melt is a mixture of both target and projectile, the solution intruding the fracture system contains material from both the target and the projectile. Thus, the process can be viewed as donation of material from the projectile to the target material. Amalgamation of projectile into the target is supported by the analysis of the projectiles used in my experiments. Those elements that were present in high concentrations in the impactor relative to the concentration of those element in the target were found to be significantly enriched. This suggests that the material that caused the enrichment was donated by the impactor.

As the excavation phase of the cratering process begins, ejecta fragments containing melted intrusions of projectile material solidify, trapping the enrichment forever in the frozen minerals. Thus, the chemical signature left after impact is an increase in the concentration of trace elements found in the projectile by amalgamation with the target material via melt/solid boundaries during the contact/compression and excavation stages.

Depletion can be explained by the vaporization and subsequent transport away from the impact site by the atmosphere. The observations and data are consistent with this hypothesis because the elements that were depleted were all moderately volatile.

During and shortly after the excavation stage of the impact process, melts of varying sizes can be found in the ejecta. Some very small melt systems are found throughout the ejecta, interspersed with un-melted minerals. As shock and rarefaction waves pass through target material, the bonds between atoms in the crystalline structure of a mineral are deformed severely and may break. Depending on the partitioning coefficient, atomic radius, electron structure, and

compatibility with the surrounding environment, ions preferentially move into and out of the melt system from the surrounding minerals. The impactor is melted by the same processes that cause melting of the target rocks. Melt from the target mixes with melt from the projectile. If conditions are right, substitution of projectile material into the crystalline structure of the target material may take place. I believe that further research will find evidence that will lead to refinement of my model.

My data support this model because melts are seen with intruded fracture systems caused by the extreme pressures of the impact event, and because the distribution of the concentration of specific elements in the experimental specimens was strongly skewed, indicating that the intensity of the chemical changes can be expressed as a function of distance from the point of impact.

Conclusion and Further Research:

Based on both chemical and physical data, I propose that partial melting of both the impactor and target material create a melt system in which some atoms and ions are mobile, resulting in enrichment of some elements in the target material. A melt mixture of target and projectile melt intrudes fracture systems formed by the passage of the shock wave(s). Depletion can be explained by vaporization of target material and/or the projectile followed by transport via atmospheric processes away from the impact site. The kinetics and thermodynamics of chemical aspects of the impact process can be described in part by a model wherein a melt composed of both target and projectile material is distributed throughout the target via melt/solid boundary interactions.

Although other processes are also likely at work, my model is an important contribution to the puzzle of the chemistry of the impact process.

The model I proposed makes some testable predictions. Firstly, it predicts that the anomalous concentrations of certain elements will be found not evenly spread throughout the target, but rather concentrated in the melts. In order to test this hypothesis, I am using an ion microprobe to determine the trace chemical composition of minerals and melts at different places throughout the experimental and control thin sections. I am also trying to arrange more impacts, this time using glass projectiles to confirm the prediction that the type of chemical signature left by an impact event is indeed dependent on the composition of the impacting body.

References:

- [1] Bland, Phillip A., et al. An Introduction to the Solar System. Ed. Neil McBride and Iain Gilmour. Cambridge: Cambridge University Press, 2004.
- [2] De Pater, Imke, and Jack J. Lissauer. Planetary Science. Cambridge: Cambridge University Press, 2001.
- [3] Ebel, Denton S., and Lawrence Grossman. "Spinel-bearing spherules condensed from the Chicxulub impact-vapor plume." Geology 33.4 (Apr. 2005): 293-296.
- [4] French, Bevan M. Traces of Catastrophe. Houston: LPI, 1998.
- [5] Koeberl, Christian. "Using Geochemical Observations to Constrain Projectile Types in Impact Cratering." Results of the Workshop on Impact Cratering: Bridging the Gap between Modeling and Observations. LPI, 2003. Lunar and Planetary Institute. 5 Apr. 2005 <<http://www.lpi.usra.edu/publications/reports/CB-1162/CB-1162-fullreport.pdf>>.
- [6] McNab, David, and James Younger. The Planets. New Haven: Yale University Press, 1999.
- [7] Melosh, H. J. Impact Cratering: A Geologic Process. Oxford Monographs on Geology and Geophysics 11. New York: Oxford University Press, 1989.
- [8] - - -. The Physics and Chemistry of Impact Cratering. ESA. 8 May 2006 <http://www.rssd.esa.int/SYS/docs/ll_transfers/367448_melosh.pdf>.
- [9] Meyers, Charles. "Shock Metamorphism." Lunar Petrographic Educational Thin Section Set. NASA. 18 July 2004 <<http://curator.jsc.nasa.gov/lunar/letss/Shock.pdf>>.
- [10] Moore, David S., and George P. McCabe. Introduction to the Practice of Statistics. New York: WH Freeman, 2006.
- [11] Ohno, Sohsuke, et al. Experimental Estimation of Chemical Reaction Rate in Vapor Clouds. ESA. 24 July 2006 <http://www.rssd.esa.int/SYS/docs/ll_transfers/295418_ohno.pdf>.
- [12] Tagle, R., et al. A Non-Magmatic Iron Meteorite as Impactor for the Rochechouart Crater. LPI. 23 Mar. 2004 <<http://www.lpi.usra.edu/meetings/lpsc2003/pdf/1835.pdf>>.